THE JOURNAL OF PHYSICAL CHEMISTRY B

Article

pubs.acs.org/JPCB

Picosecond Rotational Interconversion Adjacent to a C═O Bond Studied by Two-Dimensional Infrared Spectroscopy

Hiroaki Maekawa and Nien-Hui Ge*

Department of Chemistry, University of California at Irvine, Irvine, California 92697-2025, United States

ABSTRACT: Molecular conformations around the C═O group of carbonyl compounds like ketones and aldehydes play an important role in determining their reaction properties in solutions, including reaction rate, mechanism, steric structure, and chirality of products. Investigating different rotational conformers and their rapid exchange at room temperature will provide information on the rotational barrier and insights into how different rotamers may contribute to fundamental reactions in chemistry. We applied two-dimensional infrared (2D IR) spectroscopy and polarization-dependent IR transient grating technique to the study of 4,4-dimethyl-2-pentanone in CCl_4. Spectroscopic evidence showed that the internal rotation around the single carbon−carbon bond adjacent to the C═O group takes place on a picosecond time scale. DFT calculations suggested the presence of three different rotational conformations, one eclipsed and two staggered forms. Spectral simulation utilized the stochastic Liouville equation with a three-state jump model and incorporated the polarization factors that take into account the different direction of transition dipole moment in the three rotamers. The effects of the intramolecular vibrational energy redistribution process on the waiting time dependence of the 2D absorptive spectra were also included. Through comprehensive simulation of the observed spectral features, the exchange time constants between the three rotamers were determined: 5.4 ps from the eclipsed to staggered forms and 1.7 ps for the reverse direction.

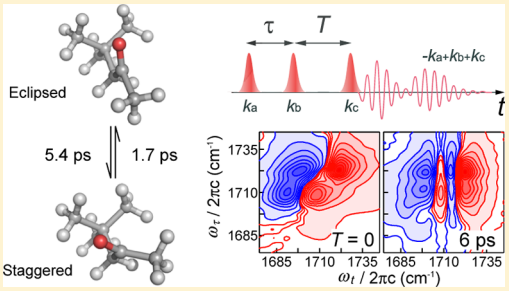

INTRODUCTION

For many chemical reactions, a double bond like C═O, C═N, and C═C is an important reaction site. Steric conformation around these functional groups plays major roles in determining reaction products, their structures, and yields.[1] This is especially true for conformationally flexible acyclic compounds, and many procedures in asymmetric synthesis have been developed to control their stereochemistry.[2] Advances in theory have been made to explain empirical selection rules of specific conformations and mechanisms, and molecular mechanical calculation has been a useful tool for synthetic strategy and molecular modeling. Further theoretical development would make it possible to discover new reaction pathways and predict regio- and stereoselectivity of more complicated compounds. To this end, detailed knowledge on the rotational isomerization process under thermal equilibrium can provide a basis to test the assumptions used in the theories and refine the torsional parameters in the force field. Available thermochemical values relevant to the millisecond rotational dynamics were obtained through dynamic NMR measurements at cryogenic temperature.[3] Most spectroscopic techniques could not directly detect conformational exchange at ambient temperature, which usually occurs on picosecond time scales. It is important to experimentally observe the isomerization process and determine the rate constant, the barrier height of the internal rotation, and steric structure of each conformation under the thermal equilibrium condition, without having to initiate it by a photo trigger, which usually probes dynamics in the electronic excited state.

Femtosecond two-dimensional infrared (2D IR) spectroscopy, a vibrational analogue of 2D NMR technique, is the ideal way to directly observe an ultrafast chemical exchange process between different species in solution phases.[4−14] It has been applied to investigate the formation and dissociation dynamics of hydrogen bonding,[4−7,12] internal rotation of substituted ethane molecules,[8] pseudorotational motion of $Fe(CO)_5$,[10] isomerization of $Co_2(CO)_8$,[11] and fast conformational switching of myoglobin.[13] In this technique, conversion between distinct states is mapped out as cross peaks located in the off-diagonal region of a 2D absorptive spectrum, consisting of the initial excitation frequency, ω_τ, and the final frequency, ω_t, detected at a fixed waiting time T. If the initial and final states are the same, and consequently the resonant frequency of a vibrational mode, peaks appear on the diagonal whose intensity decays with T due to the vibrational relaxation processes. On the other hand, if the exchange process occurs during T and the system reaches a different final state, the detected frequency becomes different from the initially excited frequency. This leads to cross peaks in the off-diagonal region of the 2D spectrum, and the rate at which their intensity grows with T can be related to the exchange rate. For example, if rotational conformers have distinct vibrational frequencies, the evolution of cross peaks can provide us with information on the rotational isomerization process. Recently, Fayer and co-workers measured the 2D absorptive spectra of 1-fluoro-2-isocyanato-

Received: June 24, 2012
Revised: August 2, 2012
Published: August 29, 2012

   dx.doi.org/10.1021/jp306201t | J. Phys. Chem. B 2012, 116, 11292−11301

ethane in carbon tetrachloride (CCl_4) at different T and estimated the rotation time constant around a carbon−carbon single bond to be 43 ± 10 ps.[8]

In this study, we aimed at observing the conformational exchange process associated with rotating a carbon−carbon single bond adjoining to a C═O group. Such a process is intimately related to nucleophilic additions to chiral carbonyl compounds.[2] Typical examples are some dialkyl ketone molecules,[15−18] such as 4,4-dimethyl-2-pentanone (DMP, Figure 1a), which can take three different rotamers in solutions:

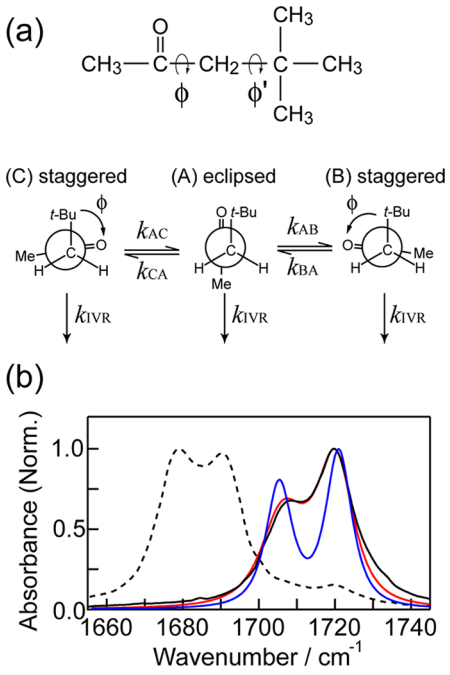

Figure 1. Rotational conformers and experimental and simulated linear IR spectra of 4,4-dimethyl-2-pentanone (DMP) in CCl_4. (a) Definition of the dihedral angles ϕ and ϕ', and the rotational conformers of DMP represented in Newman projection: eclipsed (A) and staggered (B, C). (b) Normalized FT IR spectra of DMP (black, solid) and ^{18}O-labeled DMP (black, dashed) dissolved in CCl_4. Simulated linear spectra based on the model including (red) and excluding (blue) the conformational exchange process are also shown for comparison.

eclipsed (A) and staggered (B, C).[15,16] Although the existence of several different rotational conformations in DMP and other alkyl ketones has been suggested based on FT IR measurement in several solvents,[17,18] electron diffraction measurement in the vapor phase,[19] and theoretical calculation,[20] it is still unclear how fast the conformational exchange occurs. Dielectric relaxation measurements implied that internal rotation of the ethanoyl group may occur on <10 ps time scales for some aliphatic ketones.[21,22] On the basis of the dielectric response alone, it is, however, almost impossible to specify the detailed conformations coexisting in equilibrium and to definitely distinguish internal rotational kinetics from overall molecular orientation. Polarization-dependent nonlinear IR spectroscopy can provide us with more specific structural information by measuring the transition dipole direction of a localized vibrational mode. The C═O stretching mode of carbonyl compounds is well localized and the transition dipole is almost parallel to the bond. It can be used as an ideal probe to report relative conformational differences. The rotational isomerization changes the pointing direction of the C═O mode as well as its resonant frequency, and therefore its anisotropy decay will occur along with the cross-peak evolution in the 2D IR spectra. Details of the rotational conformations and their exchange dynamics have been determined through measurement and simulation of 2D IR spectra, population relaxation, and anisotropy decay, as described below. We will also discuss the effects of intramolecular vibrational energy redistribution (IVR) on the T dependence of 2D IR spectra.

METHODS AND MATERIALS

Measurements of Nonlinear IR Signal. Details of our 2D IR spectrometer and data analysis procedure have been described elsewhere.[23,24] All of the nonlinear IR experiments were carried out using three 100 fs mid-IR pulses with wave vectors of $\boldsymbol{k}_a$, $\boldsymbol{k}_b$, and $\boldsymbol{k}_c$, centered at 1714 cm^{-1} to almost equally excite the C═O stretching modes of the different rotamers. The third-order signal emitted in the phase-matching direction $-\boldsymbol{k}_a + \boldsymbol{k}_b + \boldsymbol{k}_c$ was heterodyne detected by a local oscillator (LO) field by spectral interferometry. The polarization directions of the incident pulses and the signal (d) are denoted as ⟨abcd⟩ where IR pulses propagate approximately along the X axis of the laboratory fixed coordinates (X, Y, Z), and the Z axis was defined as the zero for polarization angles on the Y−Z plane. The zero origin of delay time was determined from the peak position of the nonresonant signal of neat CCl_4. The LO pulse preceded the signal by 800 fs.

The 2D IR spectral interferometry measurements were carried out using the rephasing (R, a-b-c) and nonrephasing (NR, b-a-c) pulse sequences. The delay times between the $\boldsymbol{k}_a$ and $\boldsymbol{k}_b$ pulses, and $\boldsymbol{k}_b$ ($\boldsymbol{k}_a$) and $\boldsymbol{k}_c$ pulses for R (NR) were defined as τ and T, respectively. In both R and NR measurements, τ was scanned from 0 to ∼6.2 ps with a time step of 9 fs at a fixed T, and the polarization configuration was set to ⟨$ZZZZ$⟩. Dispersed IR pump−probe spectra were also collected at the same delay times T and used to adjust the phase of 2D absorptive spectra based on the projection-slice theorem.[25]

The IR transient grating signal was measured using the same setup. The $\boldsymbol{k}_a$ and $\boldsymbol{k}_b$ pulses excited the sample with a zero τ delay. The decay of the population grating was monitored as the intensity change of the diffracted light from the $\boldsymbol{k}_c$ pulse as a function of T. The absolute magnitude grating signals under the ⟨$ZZZZ$⟩ polarization, $S_{ZZZZ}(T)$, and ⟨$YYZZ$⟩ polarization, $S_{YYZZ}(T)$, were measured to obtain population relaxation $p(T)$ and anisotropy decay $r(T)$ dynamics using the equations below:

$$p(T) = S_{ZZZZ}(T) + 2S_{YYZZ}(T) \quad (1)$$

$$r(T) = [S_{ZZZZ}(T) - S_{YYZZ}(T)]/p(T) \quad (2)$$

All experiments were performed at ambient temperature (20 °C).

Sample and FT IR Measurements. 4,4-dimethyl-2-pentanone (Acros Organics, 99%) was dissolved in CCl_4 (about 150 mM), and the sample solution was held in a 100 μm thick sample cell with two CaF_2 windows. An FT IR spectrum of the solution was measured with 1 cm^{-1} resolution and the average of 16 scans was taken. A background spectrum of neat CCl_4 was recorded under the same condition and subtracted from the spectrum of the ketone solution. A spectrum of the solution with ∼27-times lower concentration (about 5.5 mM) was also measured in a 950 μm thick sample

dx.doi.org/10.1021/jp306201t | J. Phys. Chem. B 2012, 116, 11292−11301

cell to check concentration dependence of the C=O stretching band. The two spectra were identical after normalization without noticeable change in intensity and peak frequency.

The ^{18}O-isotope labeling of the C=O group was achieved using the modified procedure implemented by Karabatsos.[26] Unlabeled ketone of volume 400 μL was stirred with 1 mL of $H_2{}^{18}O$ (97% ^{18}O, Cambridge Isotope Laboratories, Inc.) in the presence of a drop of sulfuric acid. The isotope exchange between ^{16}O and ^{18}O was monitored by sampling aliquot from the ketone phase and measuring the FT IR spectra of its solution film between two CaF_2 windows. Further exchange could not be observed 2 h after the stirring. *n*-Heptane (1 mL) was added to extract the isotope-labeled ketone and the solution was dried with sodium sulfate after separation from the water phase. Finally, the ketone was isolated from the *n*-heptane by distillation using a Buchi Kugelrohr apparatus. ^{1}H NMR and FT IR spectra of the unlabeled and ^{18}O-labeled DMP were measured to verify the purity.

DFT Calculation. We used a Gaussian 03 package to implement the DFT calculation for DMP in vacuum and in Tomasi's polarizable continuum model.[27] Structure optimization and normal-mode analysis were performed at the B3LYP/6-31+G(d) level at fixed dihedral angles in a step of 15° and 30° for ϕ and ϕ', respectively. The relative potential energy ΔE to the minimum energy at ϕ = 60° and ϕ' = 0° was calculated with zero-point energy correction. The same reference conformation was used to estimate the relative enthalpy ΔH and Gibbs free energy ΔG. The normal-mode frequency of the C=O stretching mode was scaled with a factor of 0.9614,[28] and the relative frequency difference $\Delta\tilde{\nu}$ from 1705 cm^{-1} at ϕ = 60° and ϕ' = 0° was calculated.

RESULTS AND DISCUSSION

Linear IR Spectra and Rotational Conformations. Figure 1b shows the FT IR spectrum of DMP dissolved in CCl_4 (black). Although the ketone has only one C=O group, two distinct peaks appear at 1720 and 1708 cm^{-1} (Table 1) as reported previously.[15,16] The origin of the doublet has been previously ascribed to the existence of different rotational conformations based on the solvent dependence of linear IR spectra.[15,16] Our FT IR measurements show that these two peaks lack concentration dependence and thus exclude the possibility of intermolecular aggregation. Moreover, we utilized isotope labeling to clarify whether the doublet peak originates from band splitting due to Fermi resonance. Isotope substitution, such as ^{13}C and ^{18}O labeling, can breach Fermi resonance interaction by lowering the frequency of the labeled mode and decoupling quasi-degenerate vibrational levels. As a result, a single band for the IR active mode would be observed upon isotope labeling. For example, a previous study has applied ^{18}O labeling to provide evidence of Fermi resonance in the C=O stretching region of cyclopentanone.[29] Figure 1b shows the FT IR spectrum of ^{18}O-labeled DMP (black, dashed). Two bands at 1690 and 1679 cm^{-1} are observed for the labeled DMP, about 30 cm^{-1} lower than the two peak positions of the unlabeled DMP. The observed frequency shift is very close to the shift of 31 cm^{-1} reported for the C=^{18}O mode of 2,4-dimethyl-3-pentanone.[26] ^{18}O isotope labeling on the C=O group also affects the absorbance ratio of the two bands. It has been reported that ^{18}O labeling significantly changes the extinction coefficient of the X = O mode (X = C, P, S, and N) in many compounds, although the reason is still not clear.[30,31] On the basis of isotope labeling and solvent and concentration dependence, we assigned the two C=O bands to different rotational conformations.

Table 1. Parameters Obtained from Measurement and Simulation of Linear and 2D IR Spectra and Results from DFT Calculation

	measurement and simulation		DFT calculation[a]	
	eclipsed	staggered	eclipsed	staggered
$\tilde{\nu}_{CO}$/cm^{-1}	1720	1708[b]	1705	1697[c]
$\tilde{\nu}_{CO(^{18}O)}$/cm^{-1}	1690	1679[b]		
$\tilde{\nu}_{2CO}$/cm^{-1}	3424	3399[d]		
transition dipole ratio	1	0.89	1	0.93[e]
Δ_0/ps^{-1}	3.0			
$2\Omega_1$/ ps^{-1}	2.9			
Ω_2/ ps^{-1}	0.70			
Λ/ps^{-1}	1.0			
$k_{AB}{}^{-1}$ ($k_{AC}{}^{-1}$)/ps	5.4			
$k_{BA}{}^{-1}$ ($k_{CA}{}^{-1}$)/ps	1.7			
Θ_{AB} (Θ_{AC})/deg	53		49[f]	
Θ_{BC}/deg	98		92[f]	
$k_{IVR}{}^{-1}$/ps	8.3			
vibrational lifetime/ps	0.67			
$D_{OR}{}^{-1}$/ps	33			
$\Delta_{CO,X}$/ps^{-1}	0.75			
ΔE/kcal mol^{-1}			0.76	
ΔE^*/kcal mol^{-1}			0.79	
ΔH_{BA}/kcal mol^{-1}	0.44[g]		0.96	
			1.4[h]	
ΔG_{BA}/kcal mol^{-1}	0.67		0.26[h]	
ΔG^*/kcal mol^{-1}			0.96	

[a]Unless noted otherwise, the DFT calculations were carried out at the B3LYP/6-31+G(d) level in continuum solvent model. [b]Peak fundamental frequency of the C=O stretching mode in the measured FT IR spectrum. [c]Frequency of the C=O stretching mode obtained from DFT normal-mode analysis and scaled by a factor of 0.9614. [d]Peak frequency of the C=O overtone band in the measured FT IR spectrum. [e]The ratio of the conformations at (ϕ, ϕ') = (0°, 60°) for the eclipsed form over that at (75°, 60°) for the staggered form. [f]Estimated for the conformations A at (ϕ, ϕ') = (0°, 60°), B at (60°, 60°), and C at (−60°, 60°). [g]Reference 16. [h]Calculated at the B3LYP/6-311++g(2d,p) level in vacuum.

To investigate the energy barriers for internal rotation and the conformations of possible rotamers, we carried out DFT calculations and normal-mode analysis [B3LYP/6-31+G(d)] in vacuum and in CCl_4 using the polarizable continuum model.[27] In the calculations, the dihedral angles ϕ for O=C—C(H$_2$)—C(—*t*Bu) and ϕ' for (O=)C—C(H$_2$)—C—C(H$_3$) were fixed (Figure 1a). The angles ϕ and ϕ' are defined as zero, respectively, when the oxygen atom eclipses with the central carbon atom of the *tert*-butyl group, and when the carbonyl carbon atom eclipses with the carbon atom of one of the three methyl groups. Figure 2a exhibits the relative electronic energy ΔE including the zero-point energy correction in the continuum solvent. The lowest energy structure is located at ϕ = 0° and $\phi' \sim$ 60°, corresponding to the synperiplanar eclipsed form. The second potential minimum is located at $\phi \sim$ 75° and $\phi' \sim$ 60°, corresponding to the synclinal staggered form. The energy difference between the two minima is $\Delta E \sim$ 0.76 kcal/mol. The potential energy acutely increases as ϕ increases toward 180° (see, for example, the slice at $\phi' \sim$ 60° indicated by red circles) when the steric hindrance between the *tert*-butyl group and the methyl group attached to the carbonyl

dx.doi.org/10.1021/jp306201t | J. Phys. Chem. B 2012, 116, 11292−11301

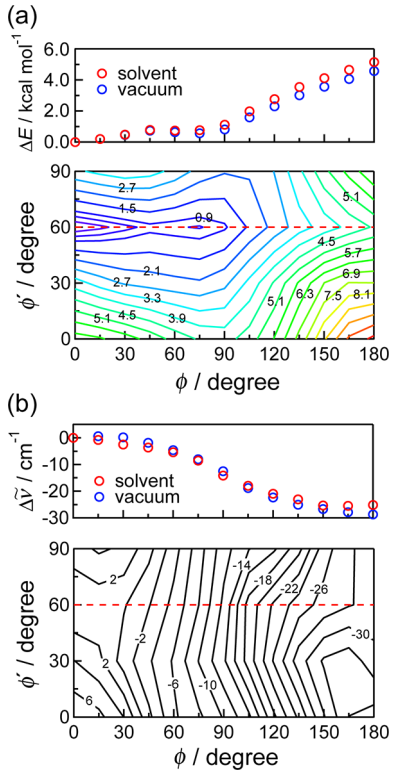

Figure 2. Results of DFT calculation [B3LYP/6-31+G(d)] implemented with a continuum solvent model. (a) A contour map of the relative electronic energy (ΔE, kcal/mol) calculated with zero-point energy correction. The minimum energy found at $\phi = 0°$ and $\phi' = 60°$ is set as the reference point of zero energy. A slice through the potential energy surface at $\phi' = 60°$ (red dashed line) is shown by red circles in the upper panel. The potential energy slice at $\phi' = 60°$ from calculations done in vacuum is also shown as blue circles. (b) The relative frequency difference of the C═O stretching mode (cm^{-1}). The scaled frequency of 1705 cm^{-1} at $\phi = 0°$ and $\phi' = 60°$ is set as the reference point of zero frequency. A slice of the frequency map at $\phi' = 60°$ (red dashed line) is shown by red circles in the upper panel. The frequency slice at $\phi' = 60°$ from calculations done in vacuum is also shown by blue circles.

group becomes significant. The shallow potential barrier between the two minima ($\Delta E^* = 0.79$ kcal/mol) and the 2-fold symmetry of the potential surface with respect to $\phi = 0$ (data not shown) suggest that three different species, one eclipsed and two staggered forms (Figure 1a), could undergo rapid conformational exchange in CCl_4 solution on a picosecond time scale. The rotation around ϕ' is 3-fold symmetric and can be ignored on this time scale because its energy barrier is greater than 4 kcal/mol for all values of ϕ.

Figure 2b shows a contour plot of the scaled C═O normal-mode frequency of DMP in the continuum solvent as a function of the dihedral angles, taking the frequency at (ϕ, ϕ') = (0°, 60°) as the reference point. Overall, the C═O frequency decreases with increasing ϕ and depends very weakly on ϕ'. The slice through $\phi' = 60°$ (red circles) indicates that the frequency of the staggered conformation is lower than that of the eclipsed conformation by about 8 cm^{-1}. A previous a priori vibrational calculation also suggested that the eclipsed form exhibits a higher frequency than the staggered form.[16] Although the two staggered forms have the same transition frequency, the different direction of the C═O group should be taken into account when simulating the 2D IR spectrum and anisotropy decay as discussed below. The angle between the transition dipole moment and the C═O bond axis is 0.5° at $\phi = 0$, and its conformational dependence is less than 5° over the whole range of ϕ.

Also plotted in Figure 2 are the relative electronic energy and vibrational frequency calculated in vacuum (blue circles). The results are similar to those calculated in the continuum solvent model. The relative energy in vacuum is slightly lower at larger ϕ and the relative frequency deviation is within ±5 cm^{-1} as shown in the slices of the surfaces at $\phi' = 60°$. We also performed two additional calculations at the B3LYP/6-311++g(2d,p) level in vacuum. The calculated vibrational frequencies for the eclipsed and staggered conformers are 1717.4 and 1710.4 cm^{-1}, respectively, with a scaling factor of 0.9679.[32]

Nonlinear Infrared Response. The T dependence of the 2D IR absorptive spectra is presented in the top row of Figure 3. At waiting time $T = 0$, two positive diagonal peaks correspond to the $v = 0 \rightarrow 1$ part of the signal from the two conformations. The two negative peaks are red-shifted from the diagonal along the ω_t axis by the diagonal anharmonicity, which is ~16 cm^{-1} for both rotamers as determined from the overtone bands at 3424 and 3399 cm^{-1} in the FT IR spectrum. Both overtone bands exhibit isotope shift upon ^{18}O labeling. No cross peaks are observed at this time because the frequency detection along the ω_t axis starts before the conformational exchange occurs. As T increases, the 2D spectral pattern shows complicated interference between diagonal and off-diagonal peaks. It becomes a square at $T = 6$ ps with two pairs of diagonal peaks and two pairs of cross peaks. An intriguing observation is that the frequency separation between the positive and negative peaks is much smaller than that at $T = 0$. This behavior is unexpected for a system undergoing simple chemical exchange.

Figure 4 depicts the schematic 2D spectral patterns of the system at different waiting times. Two conformational states, A and B, having different C═O stretching frequencies, ω^A_{CO} and ω^B_{CO}, exhibit two pairs of positive and negative diagonal peaks separated by the diagonal anharmonicities Δ^A_{CO} and Δ^B_{CO}, respectively, at early T (Figure 4a). Here we have considered the case that ($\omega^A_{CO} - \omega^B_{CO}$) < ($\Delta^A_{CO}$ and Δ^B_{CO}), in accord with our experimentally measured 12 cm^{-1} peak separation and 16 cm^{-1} anharmonicity. If the exchange process between the states occurs and hence the transition frequency changes, cross peaks between the positive or negative diagonal peaks grow as T increases, and their positions are determined by the fundamental frequency and anharmonicity (Figure 4b). For example, a negative cross peak shows up at (ω_τ, ω_t) = (ω^A_{CO}, $\omega^B_{CO} - \Delta^B_{CO}$) when a molecule transforms from the A conformer to the B conformer during T (Figure 4d). A reverse transformation from B to A would give rise to another negative cross peak at (ω_τ, ω_t) = (ω^B_{CO}, $\omega^A_{CO} - \Delta^A_{CO}$). Therefore, the negative peak that grows up after $T = 4$ ps at (ω_τ, ω_t) ~ (1720, 1713) cm^{-1} cannot be attributed to a cross peak originating from the rotational isomerization. It can most likely be explained as a relaxation-assisted cross peak between the C═O stretching mode and an accepting mode (X) that accepts the dissipated vibrational energy and is coupled with the C═O mode.[33] As the vibrational energy accumulates on the accepting mode (Figure 4e), a new negative peak would start to show up at, for example, (ω_τ, ω_t) = (ω^A_{CO}, $\omega^A_{CO} - \Delta^A_{CO,X}$) where $\Delta^A_{CO,X}$ is the cross anharmonicity between the C═O and X modes (Figure 4c). If $\Delta^A_{CO,X}$ is much smaller than the diagonal

dx.doi.org/10.1021/jp306201t | J. Phys. Chem. B 2012, 116, 11292−11301

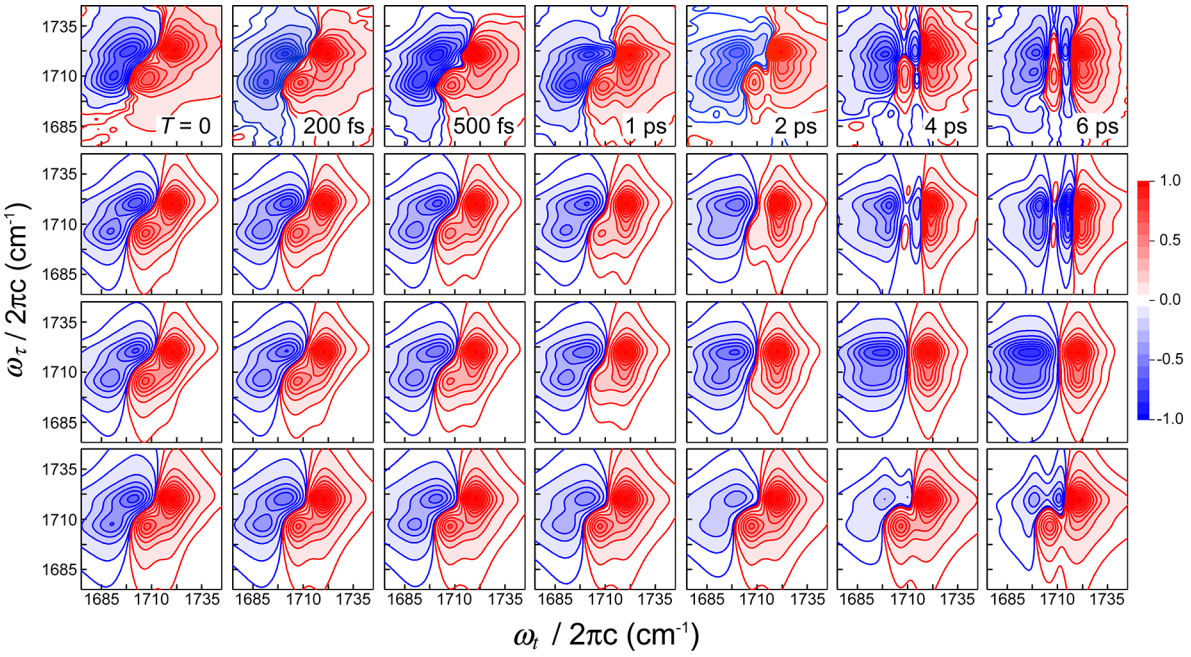

Figure 3. 2D IR absorptive spectra of DMP in CCl_4 measured with $\langle ZZZZ \rangle$ polarization at T = 0, 200 fs, 500 fs, 1 ps, 2 ps, 4 ps, and 6 ps from left to right (top). Each spectrum is normalized by the maximum amplitude of the positive peaks, and contour lines are drawn at 1.5% and from 5 to 95% of the maximum amplitude in 10% increments. The 2D IR spectra simulated based on the model including both of the conformational exchange and IVR process, only the exchange process, and only the IVR process are shown in the second, third, and bottom rows, respectively.

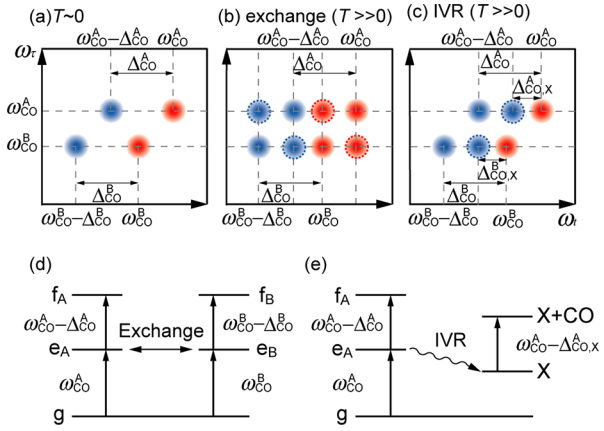

Figure 4. Schematic 2D IR spectral patterns with two different mechanisms of growing cross peaks: (a) at $T \sim 0$; (b) at $T \gg 0$ under a chemical exchange process; (c) at $T \gg 0$ under intramolecular vibrational energy redistribution. The growing cross peaks are circled with a dashed line in (b) and (c). Two different states, A and B, of the C=O stretching mode have the resonant fundamental frequencies of ω^{A}_{CO} and ω^{B}_{CO} and diagonal anharmonicities of Δ^{A}_{CO} and Δ^{B}_{CO}, respectively. An accepting mode X of dissipated vibrational energy is coupled with the carbonyl stretching mode in each state and their cross anharmonicities are represented by $\Delta^{A}_{CO,X}$ and $\Delta^{B}_{CO,X}$. They are set to be smaller than Δ^{A}_{CO} and Δ^{B}_{CO} in (c). Energy diagrams of the system with exchange process and IVR are shown in (d) and (e), respectively. In these diagrams, g, e, and f represent the ground, first, and second excited state of the carbonyl group. IVR creates vibrational population on the accepting mode X coupled with the carbonyl group, and their combination state is represented by X + CO.

anharmonicity (Δ^{A}_{CO}) and the line width of the C=O mode, this negative peak would be resolvable from the negative diagonal peak at $(\omega_\tau, \omega_t) = (\omega^{A}_{CO}, \omega^{A}_{CO} - \Delta^{A}_{CO})$. However, the line widths of the C=O modes of organic compounds are usually comparable to or larger than the anharmonicity. In this case, the position of the merged negative peak apparently shifts toward the higher frequency with increasing T, and the separation from the positive diagonal peak decreases. The simultaneous presence of chemical exchange and IVR processes leads to complex interferences between the spectral patterns in Figure 4, b and c. The growth of the positive cross peaks from chemical exchange at $(\omega^{B}_{CO}, \omega^{A}_{CO})$ becomes apparent at T = 1 ps but that at $(\omega^{A}_{CO}, \omega^{B}_{CO})$ only becomes clear at T = 6 ps because it is overshadowed by the negative diagonal peak at the earlier T. The IVR cross peak at $(\omega^{A}_{CO}, \omega^{A}_{CO} - \Delta^{A}_{CO,X})$ becomes apparent at T = 4 ps. Due to the limited spectral range, experimentally assigning the accepting mode X using our one-color 2D IR setup is difficult. Two-color 2D IR spectroscopy or IR pump and Raman probe measurement would be helpful in this regard.[33,34] Even though this IVR mechanism makes 2D spectra measured at longer T complicated, the spectral pattern is distinguishable from that of exchange only. The cross peaks in Figure 4b could not be observed if the exchange process did not occur at all. The appearance of exchange cross peaks in our 2D spectra implies that the chemical exchange due to the rotation around the C−C single bond adjacent to the C=O group takes place on time scale less than 10 ps.

Figure 5 shows the isotropic magic angle decay, $p(T)$, and anisotropy decay, $r(T)$, at 1721 and 1706 cm^{-1}, obtained from the transient IR grating measurements under the $\langle ZZZZ \rangle$ and $\langle YYZZ \rangle$ polarization configurations. The vibrational lifetime, IVR, and population exchange due to the rotational isomerization between the eclipsed and staggered forms contribute to $p(T)$. It decays within a few picoseconds followed by a tiny longer decaying component. The anisotropy starts to decay from ~0.4 and has a fast component (~1 ps) and a much slower component (>10 ps). The former is close to the orientational relaxation time of neat acetone measured by several different methods including Rayleigh scattering (0.72

dx.doi.org/10.1021/jp306201t | J. Phys. Chem. B 2012, 116, 11292−11301

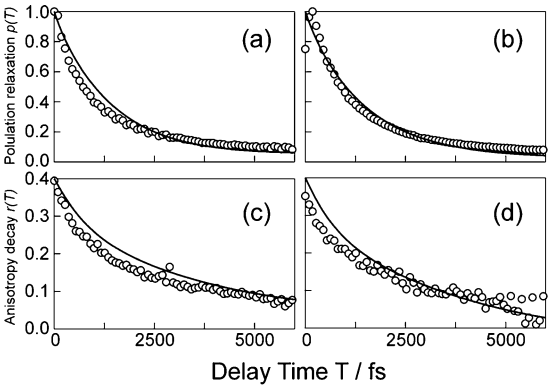

Figure 5. Polarization-dependent IR transient grating signal of DMP in CCl_4: (a, b) isotropic population decay $p(T)$ and (c, d) anisotropy decay $r(T)$. The measured signal slices at (a, c) 1721 cm^{-1} and (b, d) 1706 cm^{-1} are shown in circles. The isotropic component $p(T)$ has been normalized to the maximum value. The solid lines represent the simulated signal using the model including both the rotational exchange and IVR.

ps),[35] and IR transient grating measurement (0.75 ps).[36] However, given that the molecular volume ratio between DMP and acetone is about 1.9 and the viscosity of CCl_4 (0.908 cP) is almost 3 times as high as that of acetone (0.306 cP) at 298 K,[37] it is unlikely that the fast decaying component originates from the overall molecular tumbling. As implied from the T-dependent evolution of 2D IR spectra in Figure 3, the picosecond conformational exchange, that is, the internal rotation of the acetyl group, would induce the anisotropy decay on a similar time scale because the transition dipole direction of the C═O stretching mode changes upon conformational transition. Perhaps not incidentally, the anisotropy signal of methyl acetate in CCl_4 measured with IR pump−probe[38] has decaying components (1.1 and 17 ps) similar to those of DMP. Moreover, from dielectric relaxation measurements of alkanones and their dependence on alkyl chain length, the polar carbonyl group position, and solvent viscosity, it was qualitatively suggested that the intramolecular motion of the small polar end group makes a dominant contribution to the relaxation.[21,22] Dielectric measurements of alkyl acetates also indicate the rotation of a small motif that exhibits a fast relaxation time of 1.2−1.4 ps independent of the alkyl chain length.[39] Therefore, we attribute the fast anisotropy decay of the DMP C═O mode to internal rotation of the acetyl group and the slow component to overall orientational motion.

Theoretical Model Including Exchange Process and IVR. To quantitatively describe the chemical exchange process, the T dependence of the cross peaks needs to be extracted from the 2D IR spectra. In addition to rotational isomerization, many processes affect the spectral pattern and need to be taken into account, including IVR, vibrational dephasing, vibrational lifetime decay, and orientational motion. It has been suggested that the cross-peak volume, instead of the intensity at a single off-diagonal point, should be plotted as a function of T to properly trace the population dynamics when the presence of spectral diffusion causes changes in the line shape during the waiting time.[6] This method is not applicable here because of the presence of IVR in addition to spectral diffusion. It is not straightforward to accurately analyze the T-dependent cross-peak volumes and determine the exchange rate constants from the complicated evolution of the 2D IR spectra shown in Figure 3. Moreover, although the isotropic population dynamics and anisotropy decays obtained from IR transient grating and pump−probe experiments are often used to independently appraise the time scales for vibrational lifetime relaxation and orientational motion, it is not possible to do so in the present case. The rotational isomerization process between the two conformations of different frequencies and transition dipole directions must influence the measured isotropic and anisotropic signal decays. Therefore, all measured data ought to be simulated simultaneously in a self-consistent model. To this end, we expanded the theoretical framework by Šanda and Mukamel[9] to simulate the linear IR spectrum (Figure 1b), the T-dependent 2D absorptive spectra (Figure 3), and isotropic and anisotropic transient grating signal decay (Figure 5) using a single set of parameters.

Fundamental points of the original model based on the stochastic Liouville equations have been described in detail.[9,40] Hereafter, we briefly describe the expansion made in this study. Apart from a few exceptions, we use the same characters and symbols as in refs 9 and 40 for clarity. First, we constructed the stochastic Liouville equation using a three-state jump model, rather than the two-state jump model in the original treatment, to include three rotamers, one eclipsed and two staggered forms. As shown in Figure 1a, the conformational exchange from the eclipsed to the staggered form is described with the rate constant k_{AB} and k_{AC}, and that from the staggered to the eclipsed form is given by k_{BA} and k_{CA}. The exchange between the two staggered forms is not considered based on the much higher potential barrier for this rotation (Figure 2a). The three-state model allows us to take into account the different direction of transition dipole moment in the three rotamers and the anisotropy decay accompanied by the rotational exchange. The third-order nonlinear polarization $S^{(3)}(\tau,T,t)$ is calculated by

$$S^{(3)}(\tau, T, t) = \left(\frac{i}{\hbar}\right)^3 \theta(\tau)\theta(T)\theta(t) \langle\langle\langle I|\boldsymbol{\mu}^{(-)}\mathcal{G}(t)\boldsymbol{\mu}^{(-)}\mathcal{G}(T)\boldsymbol{\mu}^{(-)}\mathcal{G}(\tau)\boldsymbol{\mu}^{(-)}|\rho(0)\rangle\rangle_{\mathcal{H}}\rangle_{O} \quad (3)$$

The space $\mathcal{H}$ is a direct product of the vibrational, conformational, and the Brownian oscillator space, $|\rho(0)\rangle_{\mathcal{H}}$ is the equilibrium reduced density matrix, and the summing over the final states is represented by $\langle\langle I|_{\mathcal{H}}$. The Green's function $\mathcal{G}(t')$ describes the dynamical behavior during the time t' between matter−field interactions. To properly model the laser field polarization dependence, we take into account the different direction of the transition dipole of the eclipsed and staggered conformations in the dipole operator $\boldsymbol{\mu}^{(-)}$, which acts on the density matrix for each of the three field interactions. Because the molecule can switch its conformation during the time intervals between field interactions, we have to consider the population in three distinct states (one eclipsed and two staggered forms) every time the field−matter interaction occurs. For example, if a portion of eclipsed population transfers to one of the staggered states during t', the change in population is reflected in the density operator after propagating it under the Green's function $\mathcal{G}(t')$. The dipole operator $\boldsymbol{\mu}^{(-)}$ then acts on the resulting density operator to project the transition dipole in the molecular frame to electric field in the lab frame. By expanding eq 3 and taking all of the density matrix components for the possible combinations of the conformation-dependent dipole directions at the four different

interaction times, the three-state jump model properly accounts for the changes of transition frequency and dipole direction as the molecule make transitions between the different conformers. The bracket $\langle\rangle_O$ denotes the average of all orientations. For the orientational behavior of the molecule itself, the rotational diffusion model with a diffusion constant D_{OR} is considered here.[41] This treatment of field interaction and orientational averaging is essentially identical to that implemented by Khalil et al., in which they included the effects of coherence and population transfer between the symmetric and asymmetric carbonyl stretching vibrations into the orientational relaxation.[42] The complete Liouville superoperator $\hat{\mathcal{L}}_{tot}$ describing the rotational isomerization, Brownian oscillator fluctuations, and vibrational relaxation becomes

$$\hat{\mathcal{L}}_{tot} = \hat{L}_S + \hat{\mathcal{L}}_S + \hat{\mathcal{L}}_Q + \hat{\mathcal{L}}_{QS} + L_Q + \hat{L}_P \quad (4)$$

Here $\hat{L}_S$ describes the three-state-jump kinetics where the jump rates k_{AB}, k_{AC}, k_{BA}, and k_{CA} are connected by the detailed balance relation. $\hat{\mathcal{L}}_S$ represents coherent vibrational evolution that parametrically depends on the conformational state. $\hat{\mathcal{L}}_Q$ and $\hat{\mathcal{L}}_{QS}$ describe the coupling of an overdamped Brownian oscillator coordinate to the vibration that causes spectral diffusion. The latter term permits the spectral diffusion to have different magnitudes in different conformational states. L_Q is the Fokker−Planck operator that governs the Brownian oscillator dynamics. We take into account population relaxation phenomenologically through a relaxation operator $\hat{L}_P$ and employ the harmonic approximation. The transient grating signal can be described by setting $\tau = 0$ in eq 3. A matrix continued fraction method was utilized to solve the stochastic Liouville equation and obtain the Green's functions in the frequency domain.[9,43]

We include the effects of the IVR process by assuming that every conformer has one accepting mode to which vibrational energy is redistributed from the C═O stretching $\upsilon = 1$ state (Figure 4e) and the rate constant of this process is k_{IVR}. It is also assumed that the phase memory during the delay time τ is completely lost in the IVR process and hence the third-order response function for IVR is represented as a product of the linear response functions.[9] For the transition between the accepting mode (X) and its combination state with the carbonyl stretch (X + CO), the transition dipole strength and direction as well as the dephasing time are set to be the same as those of the C═O fundamental transition, assuming a weak coupling. The lifetime of the accepting mode is assumed to be much longer than the experimental time scale based on the experimental observations that vibrational cooling often occurs on the several tens of picoseconds.[44]

The ratio of transition dipole strength was estimated as $|\mu^{(A)}|:|\mu^{(B)}|:|\mu^{(C)}| = 0.89:1:1$ from the linear IR spectrum and 2D absorptive spectrum measured at $T = 0$,[5,7] assuming that the two staggered forms have the same transition strength. This ratio is close to the 0.93:1 ratio between the conformations at $(\phi, \phi') = (0°, 60°)$ and $(75°, 60°)$ obtained from our DFT calculations in the continuum solvent model. Because different rotamers have basically the same anharmonicity ∼16 cm^{-1}, the average anharmonicity parameter Δ_0 was fixed at 3.0 ps^{-1} and the conformation-dependent anharmonicity Δ_1 was set to zero. Assuming that spectral diffusion is independent of conformational and vibrational states, the parameters Δ_2, Ω_3, and Δ_3 were also set to zero. After comprehensive simulations, the following parameters were obtained: the C═O fundamental frequency difference between the eclipsed and staggered rotamers $2\Omega_1 = 2.9$ ps^{-1} (15 cm^{-1}); the relaxation rate of the Brownian oscillator $\Lambda = 1.0$ ps^{-1}, fluctuation amplitude $\Omega_2 = 0.70$ ps^{-1}; angles between transition dipoles $\Theta_{AB} = \Theta_{AC} = 53°$, $\Theta_{BC} = 98°$; the exchange rate constants $k_{AB}^{-1} = k_{AC}^{-1} = 5.4$ ps, $k_{BA}^{-1} = k_{CA}^{-1} = 1.7$ ps; $k_{IVR}^{-1} = 8.3$ ps, the $\upsilon = 1$ vibrational lifetime 0.67 ps, $D_{OR}^{-1} = 33$ ps, and $\Delta_{CO,X} = 0.75$ ps^{-1}. These parameters are summarized in Table 1 together with the vibrational properties of the molecule determined from the experiments. The simulated linear IR, 2D IR absorptive spectra, and transient grating signals are plotted in Figures 1b, 3, and 5, respectively.

The simulated 2D absorptive spectra in the second row of Figure 3 well reproduce the experimentally observed main features. The effects of the isomerization process are noticeable at around $T = 1$ ps, and the spectral patterns at longer T change significantly due to both the rotational exchange and IVR processes. For comparison, we also show the 2D spectral patterns computed using the same model but without the IVR process (the third row). The absorptive spectra still clearly depend on T and the square-shaped patterns are obtained at $T > 2$ ps. However, this model cannot reproduce the spectral details at long T at all. To illustrate the effect of IVR, we excluded the chemical exchange process from the model and slightly adjusted the homogeneous dephasing parameters in $\hat{\mathcal{L}}_Q$ to broaden the line widths for better comparisons with the experimental data. The resulting simulated 2D spectra are shown in the bottom row in Figure 3. At long T, the relaxation-assisted cross peaks appear near the diagonal and there are no cross peaks in the off-diagonal region. If both the exchange and IVR processes are excluded from the model, the simulated 2D spectrum has little T-dependence over 6 ps.

Although we cannot identify the accepting modes from our 2D IR spectra, we speculate that the modes at 1138 or 1150 cm^{-1} might be coupled with the carbonyl group, and the IVR process might involve these modes as well as other low frequency modes of the solute and solvent molecules. They are assignable to the C═O bending and CH_2 wagging motion from the DFT normal-mode analysis and are red-shifted by 2−3 cm^{-1} upon ^{18}O-isotope labeling. No experimentally determined lifetimes of these vibrational modes are available in the literature, to the best of our knowledge. Further measurements are required for a refined model of the IVR process. In a previous study of mid-IR pump and anti-Stokes Raman spectroscopy, it was conjectured that the CH_3 rocking mode of acetonitrile would have its lifetime in the range of 100−150 ps.[45] Perhaps the CH_2 wagging mode also possesses a long lifetime so that we observed vibrational transitions to the combination state between this mode and the carbonyl stretching mode.

The transient grating signals in Figure 5 are simulated quite well by our model. To ascertain the percentage of population undergoing lifetime relaxation versus IVR, we tested the situation that the entire population transfers to the accepting mode and excluded the relaxation operator $\hat{L}_P$ from the model. This test resulted in a huge offset (∼0.5) in the simulated $p(T)$ at large T, in contrast with the ∼0.07 offset observed experimentally. This behavior suggests that the ground-state bleach recovers to a large extent and only a small amount of the population (∼10%) contributes to the IVR-assisted cross peaks, as manifested by the magnitudes of k_{IVR} and $\upsilon = 1$ lifetime determined from the simulation. The simulated anisotropic

component exhibits a single-exponential decay due to the overall molecular rotation, if the exchange process is not considered.

We determined the dihedral angle ϕ of the staggered conformer by two methods. Taking the simulated angles Θ_{AB}, Θ_{AC}, and Θ_{BC} and considering the direction of transition dipole moment with respect to the C═O bond axis obtained from the DFT calculation, ϕ is determined to be ∼65°. On the other hand, the simulated frequency separation of $\Delta\tilde{\nu}$ = 15 cm^{-1} between the two rotamers corresponds to ϕ = ∼90° in the DFT map when ϕ' is fixed at 60° (Figure 2b). These two methods yield somewhat different ϕ values, suggesting room for theoretical improvement. Interestingly, the value determined by the first method is close to the value of 63° estimated from a previous a priori vibrational calculation.[16] It is noted that the simulated angles Θ_{AB}, Θ_{AC}, and Θ_{BC} are in good agreement with those obtained directly from DFT calculations (Table 1).

The Gibbs free energy difference ΔG_{BA} = 0.67 kcal/mol is determined from our simulated equilibrium constant: $k_{BA}/k_{AB} = \exp[\Delta G_{BA}/k_B T_m]$, where $\Delta G_{BA} = G_B - G_A$ with G_A and G_B being the Gibbs free energy of the eclipsed and staggered form, respectively, k_B is the Boltzmann constant, and T_m is the absolute temperature. Taking the eclipse and staggered conformations from our DFT calculations in Figure 2a, we obtained ΔG_{BA} = 0.26 kcal/mol at a higher level of theory with B3LYP/6-311++g(2d,p) in vacuum. This discrepancy indicates that a more accurate theoretical calculation including the solvent is needed to correctly predict the conformational equilibrium when the energy difference is marginal.

A common practice to extract the enthalpy change between two exchanging species has been to measure the temperature dependence of the linear IR band area ratio and construct a van't Hoff plot.[6,7,16,46] Cossé-Barbi and Massat estimated the molar enthalpy change ΔH_{BA} = 0.44 kcal/mol using this method with the band area approximately defined by the product of the maximal absorbance and the full width at half-maximum.[16] This estimate is much lower than the 1.4 kcal/mol value calculated with B3LYP/6-311++g(2d,p) in vacuum and the 0.96 kcal/mol value calculated with B3LYP/6-31+g(d) in continuum solvent. Although theoretical inaccuracy is one contributing factor for the discrepancy, the band area ratio is not a suitable measure for the relative concentration if the oscillator strength of the C═O mode depends on the steric conformation. When the measured linear spectrum was fitted with two Lorentzian functions under the assumption that $|\mu^{(A)}| = |\mu^{(B)}|$, the resulting population ratio of conformer B over A was 0.26, different from the 0.31 value obtained based on our simulated equilibrium constant. Moreover, the effects of chemical exchange on linear IR line shape and intensities would also lead to an inaccurate estimation of the band areas of the two conformations. The exchange rate constant from the staggered form to the eclipse form is relatively fast ($k_{BA}^{-1} = k_{CA}^{-1}$ = 1.7 ps) in this study. As seen in the simulated linear spectrum with the exchange process turned off (Figure 1b, blue), its influence on the linear IR spectrum is significant and the ratio of the population becomes 0.49. Thus, quantitative analysis of a coalesced band requires close attention to extract accurate information.

The potential energy for conformational exchange consists of several origins of weak interactions, for example, dipole−induced dipole interaction and the overlap of the bonding orbitals.[47] These weak interactions may be affected by solvent properties.[48] The C═O doublet of DMP has a solvent-dependent integrated area ratio,[16] which may imply different rotation dynamics in different solvents. It is natural that interactions with solvent molecules hinder the rotation and the rate in solution becomes smaller compared to that of the rotation in vacuum.

Taking the exchange rate constant k_{AB} and applying the traditional transition-state theory, we estimated the potential energy barrier (E_a) of rotational isomerization from the eclipsed to the staggered conformer to be 2.0 kcal/mol. This value is about twice the ΔG^* values, 1.0 and 0.96 kcal/mol, obtained from the DFT calculations in vacuum and continuum solvent, respectively. This discrepancy is not surprising, given that the DFT calculations underestimated ΔG_{BA}. The result once again shows the need to properly take into account the effect of the solvent.

To this end, we also applied Kramers equation[49−54] to estimate E_a:

$$k = \frac{\omega_a}{2\pi\omega_b}\frac{\beta}{2}\left\{\left[1 + \left(\frac{2\omega_b}{\beta}\right)^2\right]^{1/2} - 1\right\}\exp(-E_a/k_B T_m) \quad (5)$$

In eq 5, ω_a and ω_b are the angular frequency at the bottom of the potential well of the eclipsed conformer and at the top of the transition-state barrier, respectively. The potential is considered piecewise parabolic, with $V = \tilde{I}\omega_a^2\phi^2/2$ for the initial well. The reduced moment of inertia for the internal rotation is defined as $\tilde{I} = I_1 I_2/(I_1 + I_2)$, where I_1 and I_2 are the moments of inertia of the acetyl and CH_2-*t*Bu groups with respect to the rotational axis along the C−C bond. $\tilde{I}$, I_1, and I_2 were calculated to be 41.7, 49.6, and 259 amu Å^2, respectively. The parameter β is the rate coefficient of the decay of the angular velocity correlation. When hydrodynamic interactions are negligible, $\beta = \tilde{\xi}_r/\tilde{I}$.[50] The friction coefficient ξ_r can be described under the slip boundary condition as $4\pi\eta d r^2$ with the solvent viscosity η, the hydrodynamic radius d of a rotating sphere with the radius of gyration r from the rotation axis. Given that the acetyl group is much smaller than the CH_2-*t*Bu group and $\tilde{I} \approx I_1$, we approximate $\tilde{\xi}_r$ by the friction coefficient of the acetyl group in CCl_4 with η = 0.908 cP, r = 1.3 Å, and d = 2.2 Å, assumed to be the van der Waals radius of the acetyl moiety.[55] The angular frequency ω_a was set to 52 cm^{-1} as determined from fitting the potential well, and ω_b was obtained from the absolute value of the imaginary frequency (49 cm^{-1}) found at the transition state in the DFT vibrational analysis. This treatment resulted in 0.13 kcal/mol of E_a at 293.15 K, which is much smaller than the values estimated from the transition-state theory and the DFT calculations, and the thermal energy of 0.58 kcal/mol. Because Kramers theory is valid for systems with a large activation barrier, much higher than $k_B T_m$, the result suggests that this direct application of Kramers theory is not suitable for describing the dynamics of our system. The use of a hydrodynamic model to relate the friction coefficient to the shear viscosity of the solvent requires that the solvent is much smaller than solute in size. This assumption is not valid here since the van der Waals radius of the solvent is 5.4 Å, much larger than that of the acetyl moiety.

Previous studies showed that the rotational barrier and hence time constant depend on substitution groups on the carbon atom around which the rotation occurs.[48,56−58] For example, a theoretical study suggested that the barrier to rotation for 2-butanone (methyl ethyl ketone) has different origins from that

of ethane, and that the additional contributions result from a dipole−induced dipole interaction between the carbonyl group and the carbon−carbon bond of the ethyl group, and from the overlap of the bond orbitals of these groups.[47] In a recent study, the measured rate constant for rotational isomerization around a single carbon-carbon bond in a fluorinated ethane like molecule is 43 ps,[8] quite different from our measurement for DMP. To compare the potential energy curve of DMP to that of 2-butanone in the literature,[59] we also carried out the DFT calculation in vacuum with restraining only ϕ. The potential of DMP as a function of only ϕ is almost the same as the slice at $\phi' = 60°$ in Figure 2a. Although one alkyl substituent on the α-carbon (methyl for 2-butanone and *tert*-butyl for DMP) is the only difference between the two ketones, the calculated potential energy curves are quite different. For 2-butanone, no secondary stable conformation was found, but a broad shoulder was seen at ϕ =119°. The relative energy of this shoulder to the *trans* conformation is 1.74 kcal/mol, about 2.3 times what we computed for the staggered form of DMP. Also, the relative energy of the 2-butanone *cis* conformer at $\phi = 180°$ was 2.66 kcal/mol, about a half of that computed for DMP in this study. The comparison between 2-butanone and DMP suggests that the *tert*-butyl group in DMP induces favorable interactions for the staggered conformation of DMP, and most likely the steric hindrance becomes dominant as the two methyl groups on the *tert*-butyl moiety come close to the methyl group on the acetyl moiety when ϕ approaches 180°. Because the rotational barriers of the single carbon−carbon bond depend significantly on attached functional groups on the carbon atoms and the surrounding medium,[48] it is not unexpected that the isomerization rate constants are also different.

In summary, we have determined the rate constants for rotation around a single carbon−carbon bond adjacent to the C═O group in DMP from the measured and simulated *T*-dependent 2D IR absorptive spectra and anisotropy decay. The rotational isomerization occurs in CCl_4 with a rate constant of 0.18 ps^{-1} from the eclipsed ($\phi = 0°$) to staggered ($\phi \sim 65°$) form, and 0.59 ps^{-1} for the reverse direction. The internal rotation of the ethanoyl group changes the resonant fundamental frequency of the C═O stretching mode, and hence the dynamics of this process can be observed by monitoring the growth of the cross-peak intensity using *T*-dependent 2D IR spectroscopy. This study corroborates that picosecond rotational isomerization around the carbon−carbon bond of similar carbonyl compounds is likely to occur at room temperature, as deduced from the quite low potential barrier (∼1.5 kcal/mol) in many theoretical calculations.[20,59] *T*-dependent 2D IR spectroscopy is a very useful method to detect ultrafast exchange dynamics. The interpretation of 2D spectra can be complicated if the spectra are influenced by other processes occurring on a similar time scale. IVR is one such process and gives rise to relaxation-assisted cross peaks that grow with *T*. The presence of additional cross peaks makes it impossible to extract the exchange time constants from straightforward analysis of the spectral patterns, such as estimating the peak volumes as a function of *T*. Despite the complexity, the characteristics of the cross peaks due to the chemical exchange and IVR processes are still quite different. One can discern the patterns and extract exchange dynamics through meticulous simulation.

AUTHOR INFORMATION

Corresponding Author

*E-mail: nhge@uci.edu. Phone: 949-824-1263. Fax: 949-824-8571.

Notes

The authors declare no competing financial interest.

ACKNOWLEDGMENTS

The authors are grateful to James Nowick and Shafiullah Khan for their help in the synthesis and characterization of the ^{18}O-isotope-labeled ketone. This research was supported by grants from the National Science Foundation (CHE-0450045, CHE-0802913, and CHE-1013071).

REFERENCES

(1) Smith, M. B.; March, J. *March's Advanced Organic Chemistry: Reactions, Mechanisms, and Structure*, 6th ed.; John Wiley & Sons, Ltd.: Chichester, UK, 2007.
(2) Bartlett, P. A. *Tetrahedron* **1980**, *36*, 2−72.
(3) Binsch, G. *Top. Stereochem.* **1968**, *3*, 97−192.
(4) Woutersen, S.; Mu, Y.; Stock, G.; Hamm, P. *Chem. Phys.* **2001**, *266*, 137−147.
(5) Kim, Y. S.; Hochstrasser, R. M. *Proc. Natl. Acad. Sci. U.S.A.* **2005**, *102*, 11185−11190.
(6) Zheng, J.; Kwak, K.; Asbury, J.; Chen, X.; Piletic, I. R.; Fayer, M. D. *Science* **2005**, *309*, 1338−1343.
(7) Zheng, J.; Kwak, K.; Chen, X.; Asbury, J. B.; Fayer, M. D. *J. Am. Chem. Soc.* **2006**, *128*, 2977−2987.
(8) Zheng, J.; Kwak, K.; Xie, J.; Fayer, M. D. *Science* **2006**, *313*, 1951−1955.
(9) Šanda, F.; Mukamel, S. *J. Chem. Phys.* **2006**, *125*, 014507.
(10) Cahoon, J. F.; Sawyer, K. R.; Schlegel, J. P.; Harris, C. B. *Science* **2008**, *319*, 1820−1823.
(11) Anna, J. M.; Ross, M. R.; Kubarych, K. J. *J. Phys. Chem. A* **2009**, *113*, 6544−6547.
(12) Ghosh, A.; Remorino, A.; Tucker, M. J.; Hochstrasser, R. M. *Chem. Phys. Lett.* **2009**, *469*, 325−330.
(13) Fayer, M. D. *Annu. Rev. Phys. Chem.* **2009**, *60*, 21−38.
(14) Jansen, T. l. C.; Knoester, J. *Acc. Chem. Res.* **2009**, *42*, 1405−1411.
(15) Guillaume, P.; Massat, A.; Cossé-Barbi, A.; Dubois, J.-E. *Tetrahedron Lett.* **1980**, *21*, 1937−1940.
(16) Cossé-Barbi, A.; Massat, A. *J. Mol. Struct.* **1980**, *63*, 31−46.
(17) Hirota, M.; Hagiwara, T.; Satonaka, H. *Bull. Chem. Soc. Jpn.* **1967**, *40*, 2439−2442.
(18) Cosse-Barbi, A.; Massat, A. *Struct. Chem.* **1994**, *5*, 37−41.
(19) Abe, M.; Kuchitsu, K.; Shimanouchi, T. *J. Mol. Struct.* **1969**, *4*, 245−253.
(20) Berry, R. J.; Waltman, R. J.; Pacansky, J.; Hagler, A. T. *J. Phys. Chem.* **1995**, *99*, 10511−10520.
(21) John, C. *J. Chem. Phys.* **1972**, *56*, 2549−2552.
(22) Madan, M. P. *Can. J. Phys.* **1977**, *55*, 297−301.
(23) Maekawa, H.; Toniolo, C.; Broxterman, Q. B.; Ge, N.-H. *J. Phys. Chem. B* **2007**, *111*, 3222−3235.
(24) Maekawa, H.; Toniolo, C.; Moretto, A.; Broxterman, Q. B.; Ge, N.-H. *J. Phys. Chem. B* **2006**, *110*, 5834−5837.
(25) Jonas, D. M. *Annu. Rev. Phys. Chem.* **2003**, *54*, 425−463.
(26) Karabatsos, G. J. *J. Org. Chem.* **1960**, *25*, 315−318.
(27) Frisch, M. J.; Trucks, G. W.; Schlegel, H. B.; Scuseria, G. E.; Robb, M. A.; Cheeseman, J. R.; Montgomery, J. A., Jr.; Vreven, T.; Kudin, K. N.; Burant, J. C.; Millam, J. M.; Iyengar, S. S.; Tomasi, J.; Barone, V.; Mennucci, B.; Cossi, M.; Scalmani, G.; Rega, N.; Petersson, G. A.; Nakatsuji, H.; Hada, M.; Ehara, M.; Toyota, K.; Fukuda, R.; Hasegawa, J.; Ishida, M.; Nakajima, T.; Honda, Y.; Kitao, O.; Nakai, H.; Klene, M.; Li, X.; Knox, J. E.; Hratchian, H. P.; Cross, J. B.; Bakken, V.; Adamo, C.; Jaramillo, J.; Gomperts, R.; Stratmann, R. E.; Yazyev, O.; Austin, A. J.; Cammi, R.; Pomelli, C.; Ochterski, J. W.;

Ayala, P. Y.; Morokuma, K.; Voth, G. A.; Salvador, P.; Dannenberg, J. J.; Zakrzewski, V. G.; Dapprich, S.; Daniels, A. D.; Strain, M. C.; Farkas, O.; Malick, D. K.; Rabuck, A. D.; Raghavachari, K.; Foresman, J. B.; Ortiz, J. V.; Cui, Q.; Baboul, A. G.; Clifford, S.; Cioslowski, J.; Stefanov, B. B.; Liu, G.; Liashenko, A.; Piskorz, P.; Komaromi, I.; Martin, R. L.; Fox, D. J.; Keith, T.; Al-Laham, M. A.; Peng, C. Y.; Nanayakkara, A.; Challacombe, M.; Gill, P. M. W.; Johnson, B.; Chen, W.; Wong, M. W.; Gonzalez, C.; Pople, J. A. *Gaussian 03*; Gaussian, Inc.: Wallingford, CT, 2004.

(28) Scott, A. P.; Radom, L. *J. Phys. Chem.* **1996**, *100*, 16502−16513.

(29) Cataliotti, R.; Jones, R. N. *Spectrochim. Acta, Part A* **1971**, *27*, 2011−2013.

(30) Pinchas, S.; Samuel, D.; Weiss-Broday, M. *J. Chem. Soc.* **1962**, 3968−3974.

(31) Lapidot, A.; Pinchas, S.; Samuel, D. *J. Chem. Soc.* **1963**, 1128−1132.

(32) Andersson, M. P.; Uvdal, P. *J. Phys. Chem. A* **2005**, *109*, 2937−2941.

(33) Kurochkin, D. V.; Naraharisetty, S. R. G.; Rubtsov, I. V. *Proc. Natl. Acad. Sci. U.S.A.* **2007**, *104*, 14209−14214.

(34) Wang, Z.; Pakoulev, A.; Dlott, D. D. *Science* **2002**, *296*, 2201−2203.

(35) Dill, J. F.; Litovitz, T. A.; Bucaro, J. A. *J. Chem. Phys.* **1975**, *62*, 3839−3850.

(36) Ge, N.-H.; Zanni, M. T.; Hochstrasser, R. M. In *Ultrafast Phenomena XIII*; Miller, R. D., Murnane, M. M., Scherer, N. F., Weiner, A. M., Eds.; Springer: Berlin, 2003; pp 592−594.

(37) *CRC Handbook of Chemistry and Physics*, 88th ed.; Lide, D. R., Ed.; CRC: Boca Raton, FL, 2007.

(38) Lim, M.; Hochstrasser, R. M. *J. Chem. Phys.* **2001**, *115*, 7629−7643.

(39) Koga, Y.; Takahashi, H.; Higasi, K. *Bull. Chem. Soc. Jpn.* **1974**, *47*, 84−87.

(40) Mukamel, S. *Principles of nonlinear optical spectroscopy*; Oxford University Press, Inc.: New York, 1995.

(41) Berne, B. J.; Pecora, R. *Dynamic Light Scattering: with Applications to Chemistry, Biology, and Physics*; Dover Publications, Inc.: New York, 1975.

(42) Khalil, M.; Demirdoven, N.; Tokmakoff, A. *J. Chem. Phys.* **2004**, *121*, 362−373.

(43) Jansen, T. l. C.; Zhuang, W.; Mukamel, S. *J. Chem. Phys.* **2004**, *121*, 10577−10598.

(44) Owrutsky, J. C.; Raftery, D.; Hochstrasser, R. M. *Annu. Rev. Phys. Chem.* **1994**, *45*, 519−555.

(45) Deak, J. C.; Iwaki, L. K.; Dlott, D. D. *J. Phys. Chem. A* **1998**, *102*, 8193−8201.

(46) Klaeboe, P. *Vib. Spectrosc.* **1995**, *9*, 3−17.

(47) Wiberg, K. B.; Martin, E. *J. Am. Chem. Soc.* **1985**, *107*, 5035−5041.

(48) Orville-Thomas, W. J. *Internal Rotation in Molecules*; Wiley: New York, 1974.

(49) Kramers, H. A. *Physica* **1940**, *7*, 284−304.

(50) McCaskill, J. S.; Gilbert, R. G. *Chem. Phys.* **1979**, *44*, 389−402.

(51) Wilhelmi, B. *Chem. Phys.* **1982**, *66*, 351−355.

(52) Millar, D. P.; Eisenthal, K. B. *J. Chem. Phys.* **1985**, *83*, 5076−5083.

(53) Lee, M.; Bain, A. J.; McCarthy, P. J.; Han, C. H.; Haseltine, J. N.; A. B. Smith, I.; Hochstrasser, R. M. *J. Chem. Phys.* **1986**, *85*, 4341−4347.

(54) Barbara, P. F.; Walker, G. C. *Rev. Chem. Intermed.* **1988**, *10*, 1−33.

(55) Oishi, T.; Prausnitz, J. M. *Ind. Eng. Chem. Process Des. Dev.* **1978**, *17*, 333−339.

(56) Anderson, J. E.; Pearson, H. *Tetrahedron Lett.* **1972**, *13*, 2779−2780.

(57) John, P. L. *J. Chem. Phys.* **1969**, *51*, 832−836.

(58) Lowe, J. P. *Prog. Phys. Org. Chem.* **1968**, *6*, 1−80.

(59) Langley, C. H.; Lii, J.-H.; Allinger, N. L. *J. Comput. Chem.* **2001**, *22*, 1426−1450.